Carbon Trends 5 (2021) 100110

Contents lists available at ScienceDirect

Carbon Trends

journal homepage: www.elsevier.com/locate/cartre

One-pot synthesis of hierarchical porous carbons with extended ultramicropores: New prospective materials for supercapacitors

Analia Natali Arias[a], Jhonny Villarroel-Rocha[b], Karim Sapag[b], María Fernanda Mori[c], Gabriel Angel Planes[d,e], Victoria Flexer[a,*], Alvaro Yamil Tesio[a,*]

[a] Centro de Desarrollo Tecnológico General Savio, CIDMEJu (CONICET-Universidad Nacional de Jujuy), Palpalá, Jujuy 4612, Argentina
[b] Laboratorio de Sólidos Porosos (LabSoP), Instituto de Física Aplicada-CONICET, Dpto. de Física, Universidad Nacional de San Luis, Ejército de los Andes 950, San Luis 5700, Argentina
[c] Instituto de Investigaciones en Catálisis y Petroquímica - CONICET - Facultad de Ingeniería Química, Universidad Nacional del Litoral, Santiago del Estero 2829, Santa Fe S3000AOM, Argentina
[d] Facultad de Ciencias Exactas Fisicoquímicas y Naturales, Universidad Nacional de Río Cuarto, Ruta Nac. 36, Km 601, Río Cuarto, Córdoba, Argentina
[e] Instituto de Investigaciones en Tecnologías Energéticas y Materiales Avanzados (IITEMA), Universidad Nacional de Río Cuarto, Ruta Nac. 36, Km 601, Río Cuarto, Córdoba, Argentina

ARTICLE INFO

Article history:
Received 7 July 2021
Revised 6 September 2021
Accepted 13 September 2021

Keywords:
Porous carbons
N-doping
Hierarchical porosity
Melamine
Symmetrical supercapacitor

ABSTRACT

A series of carbon electrodes was synthesized via a modification of the polymerization-condensation reaction, where a 4:1 mass excess of melamine was added in basic media to the resorcinol/formaldehyde classical mixture. Melamine, together with variations of the pyrolysis temperature play a key role to define the chemical and textural properties of these carbons. A high nitrogen content, ranging from 23.2 to 11.3 % was determined. A low degree of crystallinity and disordered internal structure were assessed, while a hierarchical porous structure was stablished for all samples, including an important ultramicroporosity, with pore sizes below 0.7 nm. All electrodes showed a predominant double layer capacitive behaviour in aqueous H_2SO_4, while a small pseudocapacitive contribution was also evidenced for the three carbons pyrolysed at higher temperatures. These three electrodes show the highest specific capacitance (maximum of 153.6 F g^{-1}), and outstanding cycling over 10,000 cycles. A comprehensive analysis correlating morphological and surface properties and the electrochemical behaviour was carried out. The best performing carbon was selected to construct a symmetrical device for which a specific capacitance of 103 F g^{-1} was determined, reaching energy and power density values of 1.4 Wh Kg^{-1} and 111.7 W Kg^{-1}, respectively.

1. Introduction

Electrochemical capacitors, often called supercapacitors [1], have attractive characteristics such as high power density, long life cycle and fast charge-discharge rate; whereby they become promising energy storage devices [2]. According to the energy storage mechanism, electrochemical capacitors can be classified into pseudocapacitors, electric double layer capacitors (EDLCs), and hybrid capacitors [3]. Pseudocapacitors store charge by a faradaic mechanism, *i.e.* via fast oxidation-reduction reactions, and intercalation mechanisms [4]. In EDLCs, capacitance is based on the accumulation of charge at the electrode-electrolyte interface, which is due to diffusion of ions from the bulk of the electrolyte into the pores of electrodes, most often carbonaceous materials. For these devices a capacitive (non-faradaic) storage mechanism predominates [5]. However, in EDLCs there may be an additional pseudocapacitive contribution to the total capacitance which is due to the presence of surface functional groups of heteroatoms in carbonaceous electrodes, such as nitrogen [6], oxygen [7], boron [8], amongst others. Finally, hybrid capacitors, consist of one carbonaceous electrode with a predominant non-faradaic mechanism, and a second electrode based in a faradaic material; therefore, both charge storage mechanism coexist [4,5].

Evidently, the electrode material is a key component to define the storage mechanism and upper limit of specific capacitance in electrochemical capacitors. Many porous carbonaceous materi-

* Corresponding authors.
E-mail addresses: vflexer@unju.edu.ar (V. Flexer), atesio@cidmeju.unju.edu.ar (A.Y. Tesio).

https://doi.org/10.1016/j.cartre.2021.100110

als have the necessary minimum characteristics for their application as electrode materials for EDLCs: good electrical conductivity, stable physicochemical properties, large specific surface area and fast kinetics [9–11]. A large variety of materials has been reported as prospective supercapacitors, *e.g.* carbon nanotubes [3], activated carbons [9], carbon nanofibers [12], carbide-derived carbons [13], carbon micro-spheres [14] or nano-spheres [15], graphene-based materials [16], amongst others. The carbonization of organic precursors in the temperature range of 400-1000 °C under inert atmosphere, results in materials named coal chars or biochars [17]. These have been extensively employed as electrode materials for EDLCs, not only for their characteristic properties, but also because they can be obtained by inexpensive large-scale production, in marked contrast to hard-template synthesis methods, or the preparation of nanotubes, graphene, and other complex synthetic procedures. Porous carbonaceous structures increase charge accumulation favouring electric double layer formation. Depending on their sizes, pores play important and different roles in EDLCs. Micropores and narrow mesopores are usually considered to be responsible for improving charge storage, while larger mesopores and macropores contribute to electrolyte transport and ion diffusion inside the carbonaceous structure [18]. Some researchers suggest that pore sizes smaller than solvated ion size will not contribute to ion accumulation and consequently to capacitance [19,20]. However, superior capacitance values have also been reported for porous carbon electrodes with pore sizes in the range 0.7 – 1 nm [21,22]. Such anomalous capacitance for those sub-nanometer pores broke the traditional paradigm of electrolyte ions adsorption and electric double layer formation in porous carbon materials [23]. Since publication of those reports, great attention has been given to exploring sub-nanometre porous carbons. However, a high specific surface area alone does not guarantee good specific capacitance and rate capability. Pores should be available for non-faradaic reactions to take place, *i.e.* perfusion of the electrolyte to the inside of the electrode should be possible, so that the high surface area becomes accessible to electrolyte ions [24]. Thus, a hierarchical porous structure is desirable to increase the specific surface area while facilitating ionic transport. In addition, the interconnection of the pores through channels generated mainly by the macropores is important [10].

The incorporation of heteroatoms can also improve the conductivity and electrochemical activity of carbon materials [25]. Nitrogen and oxygen doping in graphitic carbon domains can improve the wettability of materials, leading to better contact with the electrolyte [6]. For example, pyridinic/pyrrolic-type N and quinone/carbonyl-type O groups have been recognized to increase surface electroactive sites, providing additional capacitance [26] and enhancing the hydrophilicity [27]. However, it has also been reported that only when there is a predominant pseudocapacitive behaviour, a high N content is expected to be beneficial to contribute to the total capacitance [28,29]. Rao *et.al.* found that a very high N content may affect textural and intrinsic properties of the carbon and, consequently, its capacitive performance. A decrease of surface specific area and intrinsic conductivity for materials with higher N contents was reported. Thereby, the authors suggested that there should be an optimal N amount to avoid an adverse effect on textural and intrinsic properties, and consequently on electrochemical performance of carbon materials [30]. The nitrogen composition for the carbon structure is defined by the reagents and/or biomass precursors used as N source, and the synthetic strategy [31–33]. A common, versatile and inexpensive methodology consists in the pyrolysis of N-rich precursors. In this way, a homogeneous N distribution and wide variety of N-compositions are achieved [34], although, unfortunately, the development of a porous structure is not necessarily guaranteed during a simple pyrolysis. Melamine is one of the N-rich precursors commonly used, maintaining a high N content after the carbonization process [33,35]. Modification of the pyrolysis temperature most often modifies the graphitization degree, heteroatom content, and, when a porous structure is developed, the textural properties (*e.g.* specific surface area, pore volume, amongst others) of the carbonaceous structure [12,33,36,37].

Herein we report on the synthesis, material characterization, and application as electrodes for electrochemical capacitors of a series of N-containing porous carbon materials. Five different samples were obtained by a straightforward synthetic procedure, where the pyrolysis temperature is varied for the different carbons. These samples are characterized by having macropores, mesopores and abundant ultramicropores. In addition, a high N content was obtained, being pyridinic-N and pyrrolic-N, the predominant species. Although the electrochemical stability window for a water-based electrolyte is relatively narrow and consequently the energy stored is limited, aqueous systems are inexpensive and friendly to the environment, while the high ionic conductivity provides these systems with higher power density. Thus, the performance of the newly synthesized carbons as electrochemical capacitors was studied using H_2SO_4 solution as electrolyte in a classical three-electrode configuration. A predominant double layer capacitive behaviour for all samples was observed. Results showed a strong influence of the textural properties on capacitance values. While in principle the N content does not directly correlate with system performance, the N-rich chemical precursor contributes to define the textural parameters. A small pseudocapacitive contribution was observed at low scan rate only for carbons synthesized at temperatures of 800 °C and above, and it was attributed to the presence of O-species. For these electrodes, higher capacitance values, good capacitance retention with varying scan rate/discharge current, and an ultra-high stability over 10,000 cycles were registered. The best performance was delivered by the electrode pyrolysed at 900 °C. Thus, this was the material of choice to build a symmetrical device. For the two-electrode configuration, results showed a specific capacitance of 103 F g^{-1} with a 90 % of cycling stability over 2,500 cycles. The energy density takes an initial value of 1.4 Wh Kg^{-1}, and the power density was determined to be 111.7 W Kg^{-1}.

2. Experimental

2.1. Synthesis of NCC-X materials

1.0 g of resorcinol (> 99.9 %, Biopack) was dissolved in 1.6 mL of formaldehyde (40 % in H_2O, with 10–20 % methanol as stabilizer, Biopack). Then, 0.8 mL of 0.1 M Na_2CO_3 aqueous solution was added with the aim to increase the pH and promote a crosslinked polymerization. Thereafter, 10.0 g of melamine (> 99 %, Biopack) was added to the mixture, which was manually stirred until a homogeneous dispersion was obtained. The mixture was kept in stove at 100 °C for 24 h, where the polymerization takes place and a light red resin is formed. The final carbonization process was carried out in a tubular furnace (T150, Indef, Argentina) under a constant N_2 flow. A heating rate of 1 °C min^{-1} was used until reaching the final temperature, which was maintained for 1 h. Five different final carbonization temperature values were used: 700, 750, 800, 850, and 900 °C. Thus, five different carbons were obtained, which were named NCC-700, NCC-750, NCC-800, NCC-850 and NCC-900, denoting the final carbonization temperature. After the carbonization time is completed, the solid materials, obtained as monoliths, were naturally cooled inside the tubular furnace until they reached room temperature. Finally, the carbon samples were ground in a planetary ball-mill (PM-100, RETSCH, Germany) at 300 RPM for 1 h until a homogeneous powder was obtained. The synthetic procedure is schematized in Fig. 1.

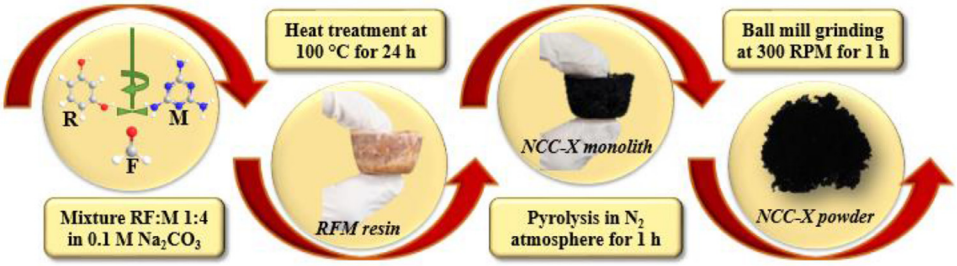

Fig. 1. Schematic representation of the 2-heating steps synthetic process for the NCC-X carbons from resorcinol (R), melamine (M), and formaldehyde (F).

2.2. Structural and chemical characterization of NCC-X materials

The microstructure and morphology of samples were determined by scanning electron microscopy, SEM (ZEISS- EVO 10 scanning electron microscope, equipped with a LaB_6 filament, UK). The images were taken using a secondary electrons detector and with an accelerating voltage of 10 kV. The crystallographic structure of the materials was investigated by X-ray diffraction, XRD (Bruker-D8 X-rays diffractometer, UK, using copper anode: Cu-Kα_1 radiation and $\lambda = 1.54056$ Å). The spectra were recorded over a 2θ range from 5° to 90° with a step of 0.026° and a scanning rate of 4° min^{-1}.

The textural characteristics of the carbons were obtained by N_2 adsorption-desorption isotherms, which were determined at 77 K (Quantachrome- Autosorb iQ gas sorption analyzer, USA). The samples were previously degassed at 280 °C for 12 h. The specific surface area (S_{BET}), taking into account the criteria recommended by IUPAC [38], was determined by the Brunauer, Emmett and Teller method [39]. The micropore volume ($V_{\mu P}$) was calculated by the α_S-plot method using the non-porous carbon Cabot BP 280 [40] as reference material. The total pore volume (V_{TP}) was estimated at relative pressure of 0.98. The mesopore size distribution was obtained by Villarroel-Barrera-Sapag (VBS) method for cylindrical pore geometry [41] using the N_2 adsorption branch data. Furthermore, the presence of narrow micropores (pore sizes less than 0.7 nm) was assessed by CO_2 adsorption isotherms at 273 K, up to 1000 kPa (Micromeritics- ASAP 2050 gas sorption analyzer, USA). From the CO_2 adsorption data the narrow micropore volume ($V_{\mu P\text{-}CO2}$) was estimated by the Dubinin-Radushkevich (DR) method and the micropore size distribution was evaluated by Horváth-Kawazoe (HK) method for slit pore geometry [42].

The surface chemical composition of the samples was determined by X-ray photoelectron spectroscopy, XPS (SPECS Multitechnique spectrometer, Germany, equipped with a dual X-ray source, Mg/Al and a PHOIBOS 150 hemi-spherical analyser in fixed analyser transmission mode, FAT). The samples were heated for 10 min at 150 °C under Ar, and then in high vacuum for at least two hours before measurements. The spectra were obtained with a step energy of 30 eV with an anode of Mg at 200 W. The pressure during measurements was less than 10^{-9} mbar. All spectrums were fitted to Gauss–Lorentz curves in order to identify the different functional groups in each material.

2.3. Electrode preparation and electrochemical test

The electrochemical performance for all carbon electrodes was evaluated by cyclic voltammetry (CV), galvanostatic charge-discharge (GCD), and electrochemical impedance spectroscopy (EIS) using a multichannel potenciostat-galvanostat (BioLogic-VMP3, France). All electrochemical measurements were performed at room temperature (19 ± 3 °C). For experiments reported in Figs. 3–9, those shown in S.I., and calculations reported in Table 2, the electrochemical measurements were conducted using a three-electrode system in a 0.5 M H_2SO_4 aqueous electrolyte. The carbon samples were used as working electrodes. A platinum mesh (1 × 1 cm^2), and Ag/AgCl electrode (in 3 M NaCl, solution BASi) were used as counter and reference electrodes, respectively. For the preparation of working electrodes, approximately 4 mg of carbon were mixed with 15 µL of perfluorinated resin solution (Sigma Aldrich- Nafion™, containing 5 wt. % in a mixture of lower aliphatic alcohols and 45 wt. % water) and 1 mL of ultrapure water. The mixture was homogenized in an ultrasonicator for 15 min. After that, 10 µL of the as-prepared homogeneous dispersion was deposited on a glassy carbon electrode (3 mm diameter, BASi), and it was let to dry at room temperature for 24 h. Cyclic voltammograms at different scan rates and galvanostatic curves at different current densities were registered in a potential range of 0.1-0.6 V. Electrochemical impedance measurements were acquired with a frequency range of 50 mHz to 100 KHz.

For experiments reported in Fig. 10, galvanostatic charge-discharge measurements were performed on a symmetric device (two-electrodes setup), using 3 M H_2SO_4 solution as electrolyte. For the two-electrode system, the working electrodes were prepared by depositing 100 µL of the as-prepared slurry for the NCC-900 material on graphite sheets (the loading mass of electroactive material is the same on both electrodes). The pre-coated graphite sheets were dried in an oven at 100 °C for 6 h. The system was assembled facing the two electrodes separated by a fiberglass paper (FilterLab MFV1, Filtros Anoia, Spain, thickness = 260 µm).

The values of specific capacitances in the three-electrodes system are calculated from CV curves based on Eq. (1) [30]:

$$C_{specific}\left(F\ g^{-1}\right) = \frac{\int I * V * dV}{m * \nu * \Delta V} \quad (1)$$

where I (A) and V (V) are the measured current and potential respectively, m (g) is the mass of active material deposited on the glassy-carbon electrode, ν (V s^{-1}) is the scan rate, and ΔV (V) is the potential window. The integral is over the enclosed area considering the charging branch from the CV curve.

The specific capacitances can also be obtained from GCD curves using Eq. (2):

$$C_{specific}\left(F\ g^{-1}\right) = \frac{I}{m * {}^{\Delta V}/_{\Delta t}} \quad (2)$$

where I (A) is the applied constant current, ${}^{\Delta V}/_{\Delta t}$ (V s^{-1}) is the slope of the discharge curve taking into account the potential window and discharge time.

For the two-electrodes configuration, the device capacitance, C_{SC}, can be calculated following Eq. (3) [43]:

$$C_{SC}\left(F\ g^{-1}\right) = \frac{I}{M * {}^{\Delta V}/_{\Delta t}} \quad (3)$$

Then, considering $m = M/2$, where M (g) represents the total mass of active material on the 2 electrodes, the specific capacitance can

be determinate based on Eq. (4):

$$C_{specific}\left(F\ g^{-1}\right) = 2\frac{I}{M * \Delta V/\Delta t} = 2C_{SC} \quad (4)$$

With other parameters as defined for Eq. (2).

The energy density, E, and power density, P, are obtained from Eqs. (5) and (6), respectively [43]:

$$E\ \left(Wh\ Kg^{-1}\right) = \frac{C_{SC} * \Delta V^2}{7.2} \quad (5)$$

$$P\ \left(W\ Kg^{-1}\right) = \frac{E * 3600}{\Delta t} \quad (6)$$

where Δt (s) is the discharge time, ΔV (V) is the potential window, excluding the potential drop, which can be determined at the start of the discharge branch.

The equivalent series resistance, *ESR*, is defined by Eq. (7) [44]:

$$ESR = V/2I \quad (7)$$

where I (A) is the discharge current, and V (V), the potential drop.

Then, the relaxation time constant, τ_o, can be calculated from EIS and GCD results following Eqs. (8) and (9) respectively [45,46]:

$$\tau_o = \frac{1}{f} \quad (8)$$

$$\tau_o = ESR * C_{specific} \quad (9)$$

where f represents the frequency at a determined capacitance in the Bode plot.

3. Results and discussions

A one-pot, two heating steps synthetic procedure was developed for the straightforward and inexpensive preparation of porous carbonaceous materials. Resorcinol (R), formaldehyde (F), and melamine (M) were mixed in a mass relation of 1:4 (RF:M) in basic medium. The catalyst (sodium carbonate) and first heat treatment favour a complete condensation-polymerization reaction between the chemical precursors, as has largely been discussed in the literature [47]. Thus, a light red resin was obtained (RFM), which is shown in Fig. 1. Then, this resin was carbonized under a constant flow of N_2 gas. Resorcinol acts as a carbon source, while melamine acts as carbon and, mainly as a nitrogen source. The large excess of melamine was purposely selected to serve as a pore generator (melamine is only slightly soluble in the basic medium). The decision to synthesize a family of carbons by varying the final carbonization temperature was taken with the aim of modifying the total nitrogen content and the textural properties of different samples.

Fig. 2 displays the resulting diffractograms and SEM images (inset) of NCC-700 (Fig. 2.a) and NCC-900 (Fig. 2.b) samples. From the diffractograms we can observe two broad peaks. An intense peak at around $2\Theta = 26°$, and a weak peak approximately centred at $2\Theta = 43°$, corresponding to the (0 0 2) reflection plane and (1 0 0) diffraction mode of graphite respectively [6]. The peak profiles in the diffractograms for the other carbon materials (see Fig. S1) show no pronounced changes. The broadness of both peaks in the diffractograms suggests a low degree of crystallinity, *e.g.* carbons with disordered internal structure. SEM images (see Fig. S2 for the other carbons) indicate that a reticular structure, with presence of abundant interconnected macro-openings of different sizes was developed. The images can be described as 3D coral-like microstructures for all materials. The size of these interconnection, in the order of hundreds of nanometres for all samples, should be enough to guarantee the electrolyte transport within the material.

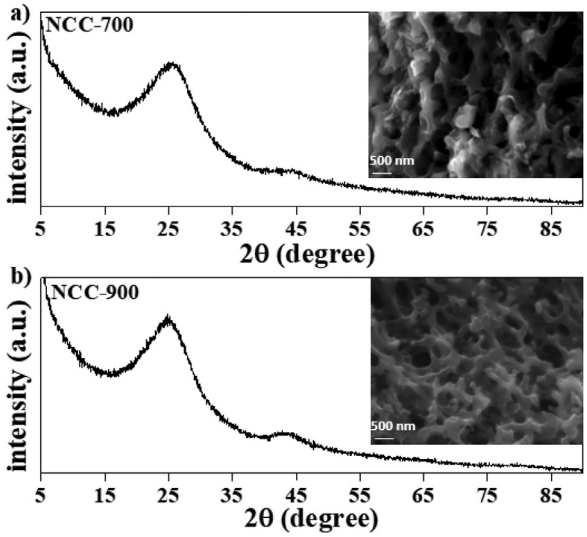

Fig. 2. Crystallographic and morphological characterization. XRD diffractograms and SEM images (inset) for: **a)** NCC-700 and **b)** NCC-900 materials.

Table 1 shows the main results obtained from gas sorption and XPS measurements. The N_2–adsorption–desorption isotherms (see Fig. S3.a), exhibit a Type I(a) isotherm according the IUPAC classification at low relative pressure, indicating the presence of narrow micropores in all materials except for the NCC-700 sample (with a very low amount of adsorbed N_2 at low relative pressure). The presence of large mesopores or narrow macropores for all carbons is also confirmed in the mesopore size distribution (see Fig. S3.b), except for NCC-850 sample, whose N_2 isotherm is different from the others with a low amount adsorbed at relative pressures close to 1. We do not have a solid hypothesis to explain the lack of large mesopores for that sample. Conversely, the behaviour of the NCC-850 carbon in the micropore region follows the trend of the other samples. From the isotherms measured with CO_2 (see Fig S4.a) the presence of narrow micropores can be confirmed. These increase in micropore size and quantity (see $V_{\mu p\text{-}CO2}$ data in Table 1) with increasing carbonization temperature. The difference in the micropore volume values obtained from measurements with N_2 and CO_2, mainly observed for the NCC-700 carbon, is due to N_2 molecules not being able to enter pores smaller than 0.7 nm. These do not allow N_2 entry because of the presence of surface groups (see below), which interact with its quadrupole moment, while this is not the case for CO_2. From the joint SEM and gas sorption analysis, we can say that all the carbons are characterized by having developed a hierarchical porosity, with pores in the ultramicro, supermicro, meso, and macroscale (0.4 nm < ultramicropore size < 0.7 nm; 0.7 nm < supermicropore size < 2 nm; 2 nm < mesopore size < 50 nm; and macropore size >50 nm) [48]. The reported dimensions of hydrated SO_4^{2-} and H^+ in sulfuric acid solution are 0.38 and 0.28 nm [49]. Thus, while their diffusion should not be hampered through the micropores, some differences in their accessibility to the micropores could be observed.

The total surface C and N compositions determined by XPS showed a clear increase and decrease respectively with increasing pyrolysis temperature. The highest N composition determined for NCC-700 sample, was of 23.9 %, while the lowest was that of NCC-900 sample, with a still quite a high value of 11.3 %. Meanwhile, the total contribution of O, remaining approximately constant, is much smaller than that both C and N (see Table S1). For C, a very clear increase in the contribution of C-C species (285 eV) can be seen, while a decrease in the C-N contribution (287 eV) follows. Meanwhile, a smaller and relatively constant contribution

Table 1
Textural properties derived from N_2 and CO_2 adsorption data, and surface elemental composition determined by XPS for NCC-X materials (% values correspond to the elemental values, *i.e.* elements indistinctly of speciation).

sample	S_{BET} ($m^2\ g^{-1}$)	$V_{\mu P}$ ($cm^3\ g^{-1}$)	$V_{\mu P\text{-}CO2}$ ($cm^3\ g^{-1}$)	V_{TP} ($cm^3\ g^{-1}$)	surface composition (XPS)		
					C (%)	O (%)	N (%)
NCC-700	73	0.01	0.13	0.15	70.8	6.0	23.2
NCC-750	420	0.11	0.17	0.37	73.7	2.3	23.9
NCC-800	505	0.14	0.18	0.34	78.8	2.6	18.6
NCC-850	400	0.12	0.18	0.19	82.1	2.8	15.1
NCC-900	410	0.12	0.20	0.28	85.4	3.3	11.3

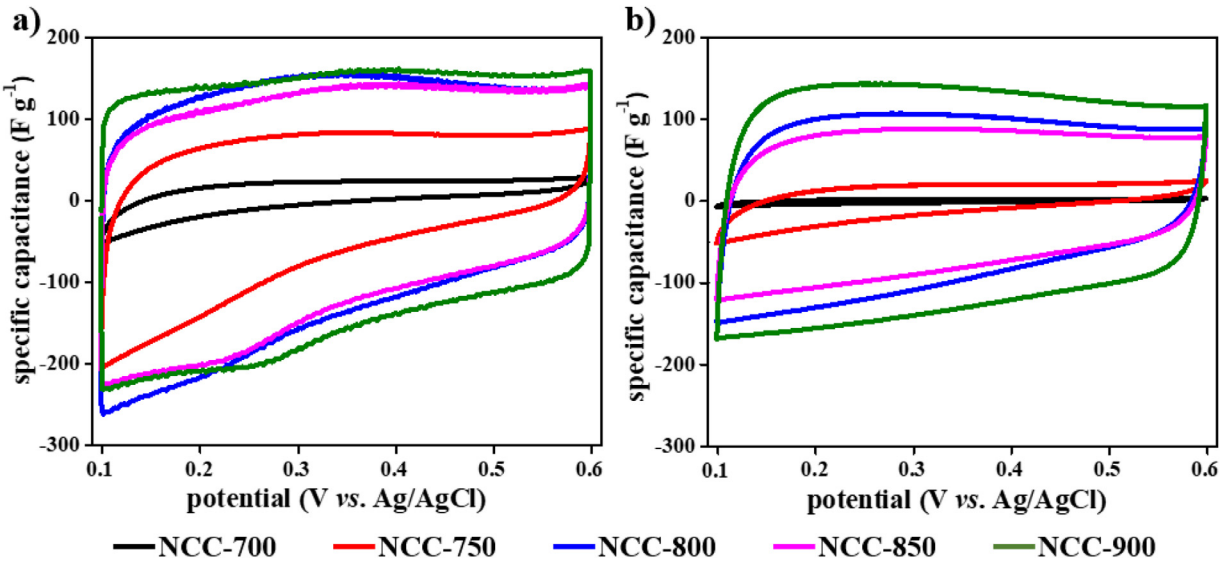

Fig. 3. Cyclic voltammograms for NCC-X electrodes in a potential range 0.1-0.6 V at scan rates of **a)** 1 mV s^{-1} and **b)** 100 mV s^{-1}. Three-electrode setup experiments and 0.5 M H_2SO_4 solution as electrolyte.

of C=O (289 eV) and COOH (291 eV) are distinguished. Regarding N, the most significant contributions correspond to the pyridinic-N (398 eV), and pyrrolic-N (400 eV) species. Conversely, the least significant contributions correspond to graphitic-N (403 eV), and oxidized-N (405 eV) species. Finally, for O smaller contributions of the N-O-C, C-O-C and C-OH species (533 eV) and COOH, C=O and N-C=O species (531 eV) are observed. The presence of N and O-based functional groups could enhance the hydrophilicity and conductivity of these carbon materials. Furthermore, these heteroatom species could be responsible for providing a pseudocapacitive contribution [26,27] (see below). As seen above, the changes to the pyrolysis temperature influence not only pore sizes and specific surface area values, but also the surface chemical composition of NCC-X materials. Based on the textural properties, it is expected that these materials possess good performance as electrodes for electrochemical capacitors.

Fig. 3 shows the CV curves for all carbon electrodes registered at scan rates of 100 mV s^{-1} (left), and 1 mV s^{-1} (right) in H_2SO_4 aqueous solution as electrolyte. Cyclic voltammograms at other scan rates are shown in Fig. S5. The main characteristic of the CV profiles for NCC-800, NCC-850, and NCC-900 electrodes at all measured scan rates is a near rectangular shape, indicating a predominant electrical double layer capacitive behaviour. In turn, for NCC-700 and NCC-750 electrodes a remarkable asymmetry is observed, particularly in the lower part of the potential window, suggesting an important resistive component in the electrochemical response. Because NCC-700 and NCC-750 samples possess smaller pore sizes (Fig S4.b), it is more reasonable to expect that the ionic transport will be limited, hindering both faradaic and non-faradaic processes. In addition, the area encircled by the cyclic voltammograms is markedly different for the different electrodes, being much larger for the group of three materials pyrolysed at higher temperatures, than for the other two. These areas already give a qualitative idea of the magnitude of the specific capacitance for the new carbons, with the highest values suggesting a better response.

Coming back to NCC-800, NCC-850 and NCC-900 electrodes, a noticeable difference in their CVs is observed when varying the scan rate. At a scan rate of 1 mV s^{-1}, weak intensity peaks for both anodic and cathodic scans are distinguishable. These peaks indicate the presence of faradaic processes (*i.e.* diffusion-controlled), leading to small pseudocapacitive contributions. Surprisingly, these peaks are not visible at a scan rate of 100 mV s^{-1}, and neither are observed for NCC-700 and NCC-750 electrodes at any scan rate. These differences suggest that diffusion-controlled processes require more time than surface-controlled ones. In addition, the pores need to be easily accessible to the electrolyte, which would not be the case for NCC-700 and NCC-750 samples. Faradaic processes are most likely due to N-containing species (mainly pyridinic-N, and pyrrolic-N), and O-containing species (particularly quinone-like and phenol-like O) [24,43], which were reported as susceptible to redox reactions with electrolyte ions [49]. We should mention, however, that it is known that contributions to pseudo-capacitance due to N-species are not always displayed in the form of redox peaks [50], as is the usual case for the well-known quinone/hydroxiquinone redox functional pair.

Fig. 4 shows the influence on the capacitance values with the increase in scan rate for two selected samples. For NCC-900 electrode, almost all curves maintained a good rectangular shape, even for the highest scan rate tested (100 mVs^{-1}), indicating a quick response for both ions and electron transport, and small polarization resistance [26]. Thereby, once again this material shows a good electrical double layer capacitive behaviour and superior rate

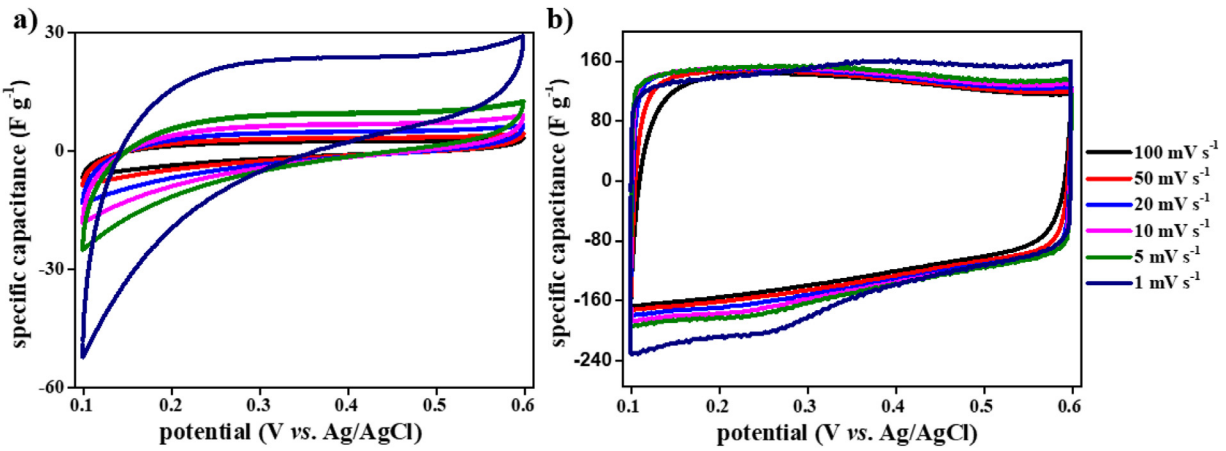

Fig. 4. Cyclic voltammogram profiles at different scan rates for: **a)** NCC-700 and **b)** NCC-900 electrodes. Three-electrode setup experiments and 0.5 M H_2SO_4 solution as electrolyte.

Table 2
Specific capacitance values calculated from cyclic voltammograms for NCC-X electrodes at different scan rates. Three-electrode setup experiments and 0.5 M H_2SO_4 solution as electrolyte.

ν (mV s^{-1})	specific capacitance (F g^{-1})				
	NCC-700	NCC-750	NCC-800	NCC-850	NCC-900
1	12.1	72.3	139.6	129.0	153.6
5	6.1	47.8	122.7	110.3	145.6
10	4.6	38.7	116.0	102.6	142.0
20	3.4	30.5	109.3	95.1	137.7
50	2.4	21.0	99.7	84.8	131.2
100	1.8	15.1	90.4	76.6	124.0

capability. Only a very slight decrease in the specific capacitance takes place with increasing scan rate, suggesting a good performance rate. Conversely, severe changes appear in the curves corresponding to NCC-700 electrode. The voltammograms tend towards high negative current values around the potential 0.1 V, which suggests an important polarization, a poor reversibility and a hampered accessibility of the ions within the pores, mainly for the discharge [24,51]. Furthermore, a quick decay in the specific capacitance takes place with increasing scan rate, indicating a poor performance rate.

In summary, according to the CV profiles both behaviours, electrical double layer and pseudo-capacitive are distinguishable. However, it should be stressed that there is a predominant electrical double layer capacitive response at the scan rates analysed. A small pseudo-capacitive contribution is discovered in some materials and lower scan rates. Finally, a non-negligible resistive response for the NCC-700 and NCC-750 materials is observed. The specific capacitance values calculated following Eq. (1) are listed in Table 2. These confirm a decrease of capacitance with increasing scan rate. The materials can be classified into two groups. The first one comprised of NCC-800, NCC-850, and NCC-900 electrodes, where higher capacitances are observed, which values change moderately with the scan rate if compared with the second group. The capacitance retention is shown in Fig. 5. A retention of 85 % is observed for NCC-900 electrode. At the other end, NCC-700 and NCC-750 electrodes, show poor capacity retention. Thinking about the porosity, at low scan rates, electrolyte ions have more time to diffuse into smaller pores producing a significant increase in specific capacitance [30]. For materials pyrolysed at higher temperatures, it would seem that the ions manage to move through the seemingly optimized pore sizes, even at relatively high scan rate values (100 mV s^{-1}).

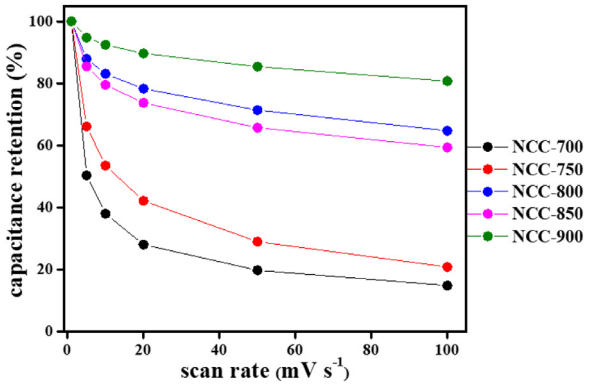

Fig. 5. Capacitance retention for all carbon electrodes at varying scan rates. Three-electrode setup experiments and 0.5 M H_2SO_4 solution as electrolyte.

Fig. 6.a compares the GCD profiles for all NCC-X electrodes at a current density of 1 A g^{-1}. The trends observed from CV curves are in agreement with observations from the GCD curves. NCC-800, NCC-850 and NCC-900 carbons present symmetrical triangular-shaped curves, suggesting a dominant electric double layer capacitive behaviour. For each specific carbon, very similar charge and discharge times indicate good electrochemical reversibility, which will be reflected in high coulombic efficiency [24,52]. In turn, if we wish to compare the different carbons, longer charge-discharge time intervals results in higher capacitance [49]. In this regard, the NCC-900 electrode possesses the largest discharge time, with a specific capacitance of 147 F g^{-1}, indicating the highest value, amongst all the newly synthesized carbons. For the NCC-700 and NCC-750 electrodes, much smaller time intervals are observed, resulting in lower capacitance values. Specific capacitances calculated by Eq. (2) are represented in Fig. 6.b (as well as listed in Table S2). As it was already mentioned, a decrease in capacitance can be linked to a limited diffusion of the electrolyte ions into the pores. The galvanostatic charge-discharge curves were measured at different current densities in order to further evaluate the ability of the electrodes to retain their capacitance with the increase in the applied current. Once again, the best results were obtained for NCC-800, NCC-850 and NCC-900 electrodes, with capacitance retentions of 69.7 %, 68.2 % and 88.2 % respectively at 20 A g^{-1} vs. capacitance values determined at 1 A g^{-1}.

Fig. 7 shows the relationships between the obtained capacitance values (determined at low scan rate, 1 mV s^{-1}, see Table 2) and some textural parameters. To evaluate the effect of pore size, the

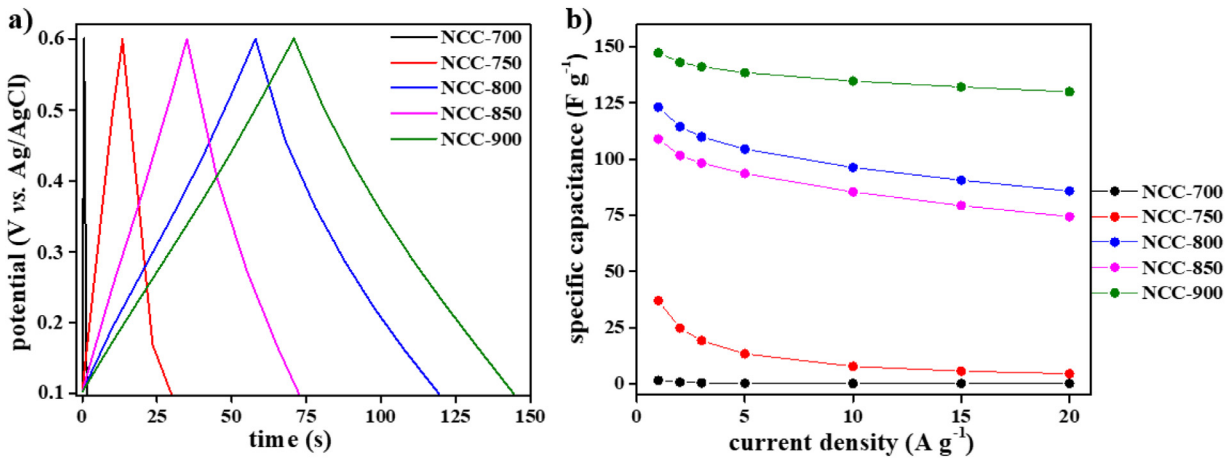

Fig. 6. **a)** Galvanostatic discharge-charge curves showing potential variation as a function of time at a current density of 1 A g^{-1}. **b)** Variation of specific capacitances with increasing current density values, for current density range of 1-20 A g^{-1}. Three-electrode setup experiments and 0.5 M H_2SO_4 solution as electrolyte, potential range of 0.1-0.6 V.

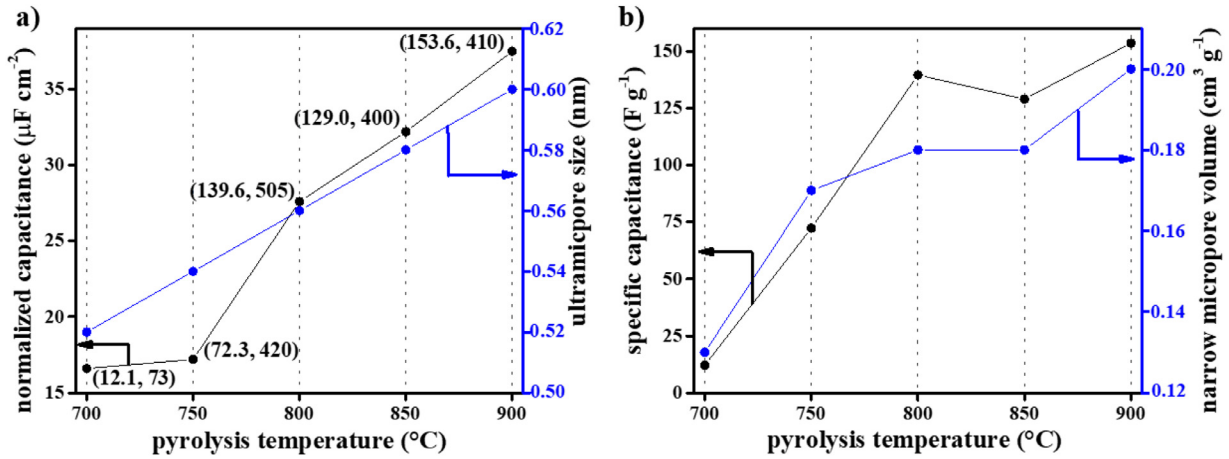

Fig. 7. Correlation of the capacitance values for the carbon samples with their textural properties. **a)** Left y-axis: normalized capacitance. Right y-axis: ultramicropore size. The values in between parenthesis next to each data point represents the specific capacitance in F g^{-1} at 1 mV s^{-1}, and the second, the S_{BET} in m^2 g^{-1}, respectively. **b)** Left y-axis: specific capacitance. Right y-axis: narrow micropore volume ($V_{\mu P\text{-}CO2}$).

specific capacitance was normalized by the specific surface area, S_{BET}. Fig. 7.a displays the correlation of normalized capacitance values and the size of the ultramicropores. For reference, in the figure the values between parentheses represent the specific capacitance at 1 mV s^{-1}, and the S_{BET} for each material. Both higher specific capacitances and normalized capacitance values are observed in those NCC-X materials characterized by having higher S_{BET}. A different behaviour is observed for the NCC-750 carbon, which presents a S_{BET} comparable to that of NCC-800, NCC-850 and NCC-900 carbons, but registers a low specific capacitance; suggesting that the developed specific surface area of NCC-750 sample is not fully accessible to electrolyte ions. We should remember that S_{BET} is estimated by gas adsorption data, which is not necessarily the same surface area electrochemically available [20]. If we overlap the curves corresponding to normalized capacitance (in black), with that for ultramicropore size (blue); the reduction in normalized capacitance for the NCC-750 electrode would indicate that the specific surface area accessible to electrolyte ions (effective area that allows for formation of the electrical double layer) is significantly smaller than S_{BET} for that specific material. This is probably due to the smaller pore sizes, that are likely to have gone below a certain critical size needed for electrolyte accessibility. In the case of the NCC-700 electrode, its low capacitance value seems to be due to both its low specific surface area and smaller pore sizes. The increase in normalized capacitance for NCC-800, NCC-850 and NCC-900 electrodes is then correlated with their larger S_{BET} and the increase in the size of the ultramicropores. Fig. 7.b shows the correlation of another textural parameter, the narrow micropore volume ($V_{\mu P\text{-}CO2}$), with the specific capacitances of the electrodes. The abundance of narrow micropores (*i.e.* ultramicropores) increases with pyrolysis temperature and it is observed that the specific capacitance tends to increase with $V_{\mu P\text{-}CO2}$. The slightly higher specific capacitance of NCC-800 electrode, as compared with NCC-850 electrode, could be explained by the almost identical narrow micropore volume, but 25 % higher specific surface area, *i.e.* larger specific surface area available for double layer formation, and micropore size already beyond the apparent minimum for adequate ion diffusion into the said pores. At this point, we should also remember that the NCC-850 electrode showed an anomalous behaviour in the N_2 sorption analysis. The absence of large mesopores could be another cause to explain a slower electrolyte diffusion, resulting in a slightly lower specific capacitance for that electrode.

A high N content was previously reported to contribute to an increase in total capacitance. However, this is the case for materials where the pseudo-capacitive is the major contribution to the total capacity [28,29,53]. In the case of the family of carbons presented here, a predominant electrical double layer capacitive be-

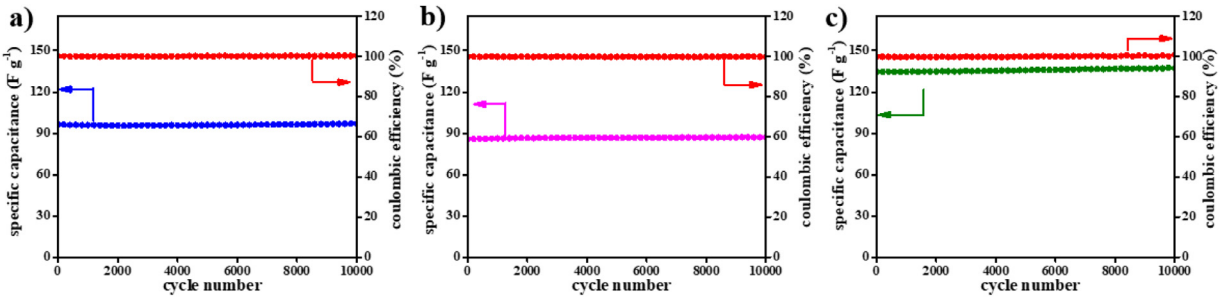

Fig. 8. Cycling stability and coulombic efficiency over 10,000 cycles at an applied current density of 10 A g^{-1} for the electrodes **a)** NCC-800, **b)** NCC-850 and **c)** NCC-900. Three-electrode setup experiments and 0.5 M H_2SO_4 solution as electrolyte.

haviour was confirmed. The nitrogen content appears not to be linked to the capacitance values, or eventually, its content would be inversely proportional to the developed capacity. We believe however that the trend in capacity values observed for the different materials is predominantly linked to the textural properties, not the surface composition. We should however remember that the nitrogen rich precursor (melamine) played a key role in the development of the porosity and the surface specific area during the pyrolysis process.

In addition to the specific capacitance and capacitance retention with increasing current density, the cyclability is another important parameter for material characterization. Fig. 8 shows the results for charge-discharge measurements over 10,000 cycles at 10 A g^{-1} performed on the NCC-800, NCC-850 and NCC-900 electrodes, *i.e.* those that previously showed the best capacitive responses. For the three carbons, ultra-high cycling stabilities were measured, with capacitance retention values slightly higher than 100 %, indicating an increase in specific capacitance in the long term. This behaviour is attributed to the continuous activation of the electroactive material during cycling, and to the uninterrupted and easier access of the electrolyte into the pores [29,54]. This extremely high capacity retention is also a strong indication that most of the capacity of these materials stems from the energy storage in the electrical double layer. Indeed, faradaic currents, are much more likely to be degraded due to irreversible chemical reactions, than ionic non-faradaic currents, only associated to ionic diffusion. With regards to coulombic efficiencies, their values around 100 % reflect the good reversibility of the systems. In Fig. 8 we also observe that the coulombic efficiencies are slightly above 100 %, which may be due to a discharge time slightly higher than the charging time in the galvanostatic curves, distorting the triangular shape. This difference between charge and discharge times can be attributed to the polarization of the electrode [55].

Fig. 9.a shows the Nyquist plots for NCC-800, NCC-850, and NCC-900 electrodes, which present similar profiles to the spectra reported for other materials that have been proposed as capacitors [9,24,26]. We can observe a semicircle in the high-intermediate frequency zone, and a line almost perpendicular to the Z_{real} axis in the low frequency zone. The semicircle represents the resistive impedance domain and it is related to charge transfer. Meanwhile, the second region, *i.e.* the vertical line represents the capacitive impedance domain and it is associated with the diffusion capacity of the ions in the electrolyte [43]. The semicircle for the high-frequency region represents the equivalent series resistance, *ESR*, which comprises the resistance of the electrolyte solution, the intrinsic resistance of the electroactive material, and the carbon-current collector interfacial contact resistance [12,51]. A smaller *ESR* value indicates a higher intrinsic conductivity and charge storage capacity in the electrical double layer [26,56]. The NCC-900 electrode shows a semicircle with a smaller diameter (see inset Fig. 9.a), indicating its better intrinsic conductivity and charge accumulation with respect to the NCC-800 and NCC-850 electrodes. For the low-frequency region, a line with an almost vertical slope indicates a good diffusion and confirms a better ideal capacitive behaviour (non-faradaic) [26,30]. The almost vertical slope is also an indication of the absence of ion diffusion limitations into the whole volume of the porous carbon structure, which would be evidenced, for example by a Warburg component [46]. Thus, the NCC-900 electrode presents the highest slope and its shorter length accounts for a higher capacitance value. The other two electrodes, with similar characteristics, present a lower slope, if compared with the NCC-900 electrode, slightly moving away from the ideal capacitive behaviour. In addition, the length of both lines is greater indicating a smaller capacitance. These results correlate very well with those obtained by CV and GCD measurements.

Fig. 9.b shows the relationship between capacitance and frequency. Already in the low frequency region, the capacitance values quickly decrease for NCC-800 and NCC-850 electrodes, while the decrease is more gradual for NCC-900 electrode. The capacitance values continue to decrease as the frequency increases, tending toward a zero value for the high frequency region for all three electrodes. This behaviour can be explained by inadequate ion diffusivity into pores [29]. Thus, for a given frequency, for example 1 Hz, the NCC-900 electrode retain up to 85 % of its maximum capacitance, while the other two electrodes only 67 % (defining the maximum capacitance as the value determined at the lowest frequency value studied). The NCC-900 electrode shows a better frequency response than the NCC-800 and NCC-850 electrodes. Alternatively, for a fixed capacitance retention, for example 50 % of the maximum capacitance, the NCC-800 and NCC-850 electrodes reach it at a frequency of 3.6 Hz, *i.e.* a relaxation time constant of 0.27 s. In contrast, the NCC-900 electrode achieves it for a higher frequency, 13.6 Hz giving a relaxation time constant of 0.07 s; showing once again a better performance.

Finally, the experimental impedance data were fitted to the equivalent circuit shown at the bottom of Fig. 9.a. This consists of solution resistance (R_s), charge transfer resistance (R_{ct}), double-layer capacitance or constant phase element (*CPE*), Warburg impedance (Z_w) and leakage capacitance or pseudocapacitive element (C). The parameter values obtained by Randomize-Simplex fitting method are shown in Table S3. Very interestingly, the pseudocapacitive values (C) obtained from the fitting are very close to the specific capacitance values obtained from the cyclic voltammograms at the lowest scan rates (see Table 2), suggesting that the chosen equivalent circuit is a good representation of the physicochemical system.

All electrochemical tests performed under a three-electrode configuration determined a better performance for the NCC-900 material. Thus, this was the material of choice to build a symmetrical capacitor, *i.e.* two- electrode configuration, which is much closer to a real device [57]. Preliminary experiments with 0.5 M H_2SO_4 aqueous solution (*i.e.* the electrolyte used in the three-

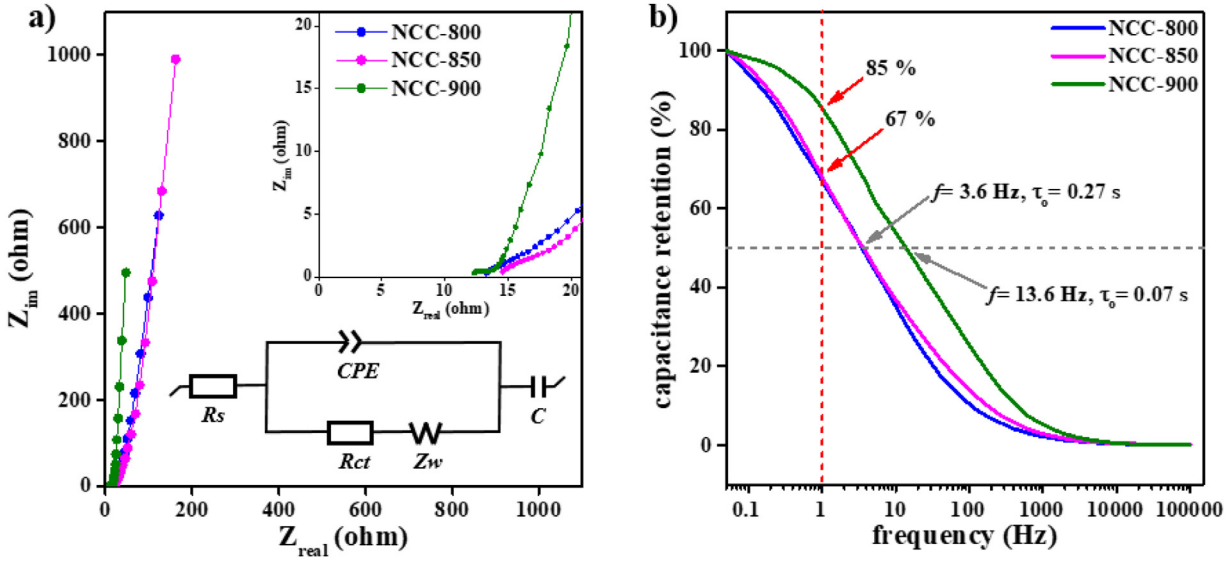

Fig. 9. Electrochemical impedance spectroscopy measurements for the NCC-800, NCC-850 and NCC-900 electrodes. **a)** Nyquist's plots. Zoom for high frequency region (inset). The equivalent circuit used is shown at the bottom of the graph. **b)** Capacitance retention as a function of frequency. Three-electrode setup experiments and 0.5 M H_2SO_4 solution as electrolyte.

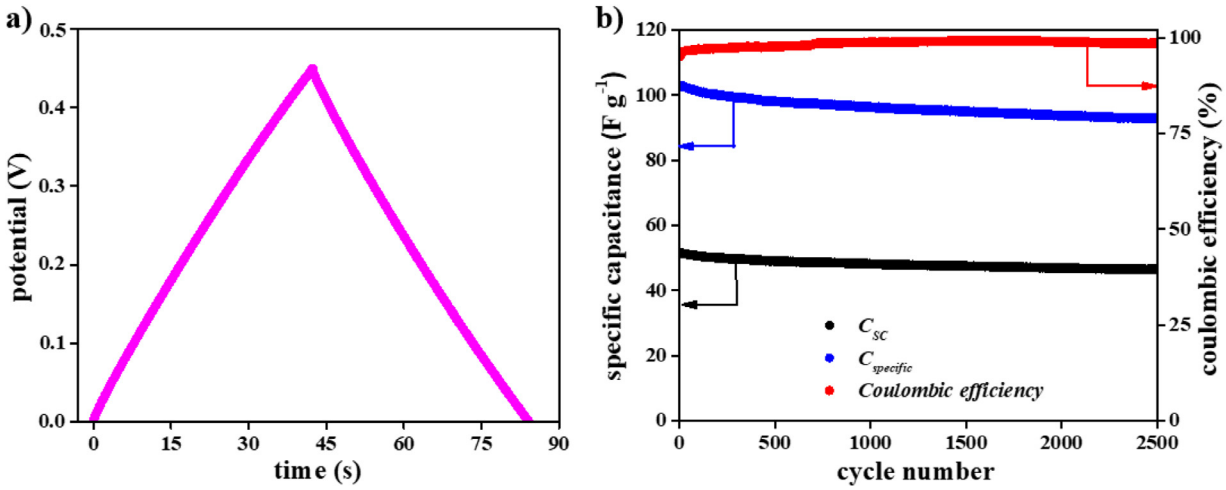

Fig. 10. Galvanostatic charge-discharge for a symmetric capacitor (*i.e.* two electrode setup) at a current density value of 1 A g^{-1} on a potential range of 0-0.45 V in 3 M H_2SO_4 electrolyte. **a)** Variation of potential as a function of time. **b)** Specific capacitance values, calculated both as C_{SC} and $C_{specific}$, and coulombic efficiency values for continuous 2500 cycles.

electrode experiments) showed GCD curves which were not symmetrical (see Fig. S6), and consequently a low coulombic efficiency. Those results suggested that in a configuration where the availability of electrolyte is limited (the separator has only been soaked in electrolyte) the availability of ions limits performance. Hence, a higher ionic concentration was needed, to facilitate ionic transport and to guarantee formation of an effective electric double layer [58]. Next, experiments were repeated using 3 M H_2SO_4 aqueous solution as electrolyte. Fig. 10.a represents the galvanostatic charge-discharge response for an applied current density of 1 A g^{-1}, for the symmetrical capacitor built with two identical NCC-900 electrodes. The curve shows a symmetrical triangular shape, which indicates that the electrode achieves good electrochemical reversibility and excellent coulombic efficiency under the experimental conditions. Fig. 10.b shows the stabilities at 1 A g^{-1} and over 2,500 cycles of device capacitance, C_{SC}, the single electrode capacitance, $C_{specific}$, and the coulombic efficiency. Considering the $C_{specific}$ value calculated by Eq. (4), for the initial cycle, $C_{specific}$ is about 103 F g^{-1}. While for the final cycle, it registers a value of 93 F g^{-1}, representing a 90 % of the initial capacitance. This indicates that the device exhibits excellent capacitance stability over the cycling process. The difference between the specific capacitance values obtained from three- and two-electrode systems (147 F g^{-1} and 103 F g^{-1}, respectively) is easily explained by a slightly different potential window, different electrode mass per current collector area, and thus thickness, and cell construction parameters, most importantly, the limited electrolyte volume and the presence of a separator [59]. Regarding the coulombic efficiency, it starts with 95 % and increases with the increase in the number of cycles, reaching 98.5 % in the final of cycling.

The *ESR* calculated from GCD curves and using Eq. (7) is 4.3 Ω, indicating a low potential drop (approximately 4 mV) due to the change in polarity ($I_{(-)} \leftrightarrow I_{(+)}$). The relaxation time constant, calculated according to Eq. (9), indicates a value of 0.4 s for the initial cycle, *i.e.* a fast frequency response of the NCC-900 electrode. A small *ESR* value results in a small τ value and, consequently, a better power density is expected [45]. Considering the initial C_{SC} value, the calculated energy density is of 1.4 Wh Kg^{-1} and the

power density equals 111.7 W Kg^{-1}. These power and energy values place the device prepared with NCC-900 carbon within the zone belonging to supercapacitors or electrochemical capacitors in a classical Ragone plot (see Fig. S7) [4].

4. Conclusion

A family of carbons with hierarchical porosity and high nitrogen content were synthetized by a versatile and inexpensive one-pot, two heating steps process. Resorcinol, formaldehyde and excess melamine in basic medium undergo a polymerization-condensation reaction, and the resulting resin is pyrolysed under inert atmosphere, developing an interconnected 3D porous structure. The nitrogen-rich precursor played an important role to generate the porous structure. Moreover, a high N content in the final electrodes, going from 23.2 % down to 11.3 % was found. Differences in textural parameters and chemical compositions were achieved varying the final pyrolysis temperature.

When the newly synthesized porous carbons were tested as electrochemical capacitors, all samples showed a predominant electrochemical double layer capacitive behaviour. The electrodes obtained from pyrolysis at temperatures 800 °C and above showed a small pseudocapacitive contribution at slow scan rates. Furthermore, these were the materials that exhibited highest specific capacitances, a good capacity retention with discharge rate, and outstanding cycling over 10,000 cycles, characteristics that are attributed to narrow micropore volume, pore sizes and accessible electrochemically specific surface area. The carbon obtained from pyrolysis at 900 °C (NCC-900) delivered the highest specific capacitance (approximately 150 F g^{-1} at 1 A g^{-1}) and excellent rate capability (about 88 % of capacitance retention when current density increases to 20 A g^{-1}), indicating a good accessibility into its smaller pores. Finally, a symmetrical capacitor with two identical NCC-900 electrodes was constructed, and these showed a device capacitance around the 50 F g^{-1}.

Declaration of Competing Interest

The authors declare that they have no known competing financial interests or personal relationships that could have appeared to influence the work reported in this paper.

CRediT authorship contribution statement

Analia Natali Arias: Formal analysis, Investigation, Methodology, Writing – original draft. **Jhonny Villarroel-Rocha:** Investigation, Methodology. **Karim Sapag:** Conceptualization, Supervision, Writing – review & editing. **María Fernanda Mori:** Formal analysis, Investigation. **Gabriel Angel Planes:** Supervision, Writing – review & editing. **Victoria Flexer:** Conceptualization, Writing – review & editing, Supervision, Funding acquisition. **Alvaro Yamil Tesio:** Conceptualization, Supervision, Writing – original draft, Writing – review & editing, Funding acquisition.

Acknowledgment

Sistema Nacional de Microscopías and ANPCyT are gratefully acknowledged for the XPS analysis carried out on the SPECS multitechnique analysis instrument (PME8-2003), and the SEM analysis carried out on the Carl Zeizz EVO-MA10 (Jujuy). ANA acknowledges a doctoral fellowship from CONICET, JV-R, KS, MFM, GAP, AYT, and VF are permanent research fellows from CONICET. Funding through PROICO 2018 N°3-2-318 from UNSL, PIP 112-201301-00832 CO 2014 from CONICET, and the project “A highly versatile selective approach for lithium production" by the Royal Society (IC170232) are gratefully acknowledged. XRD tests were performed at INQUIMAE (UBA-CONICET).

Supplementary materials

Supplementary material associated with this article can be found, in the online version, at doi:10.1016/j.cartre.2021.100110.

References

[1] J. Conder, K. Fic, C.Matei Ghimbeu, 10 - Supercapacitors (electrochemical capacitors), in: M. Jeguirim, L. Limousy (Eds.), Char and Carbon Materials Derived from Biomass, Eds., Elsevier, 2019, pp. 383–427.
[2] M.C. Liu, L.B. Kong, P. Zhang, Y.C. Luo, L. Kang, Porous wood carbon monolith for high-performance supercapacitors, Electrochim. Acta 60 (2012) 443–448.
[3] K.S. Kim, S.J. Park, Synthesis and high electrochemical capacitance of N-doped microporous carbon/carbon nanotubes for supercapacitor, J. Electroanal. Chem. 673 (2012) 58–64.
[4] K.Sharma Poonam, A. Arora, S.K. Tripathi, Review of supercapacitors: materials and devices, J. Energy Storage 21 (2019) 801–825.
[5] J. Zhao, A.F. Burke, Review on supercapacitors: Technologies and performance evaluation, J. Energy Chem. 59 (2021) 276–291.
[6] Y. Zheng, H. Wang, S. Sun, G. Lu, H. Liu, M. Huang, J. Shi, W. Liu, H. Li, Sustainable nitrogen-doped carbon electrodes for use in high-performance supercapacitors and Li-ion capacitors, Sustain. Energy Fuels 4 (4) (2020) 1789–1800.
[7] L. Xia, H. Huang, Z. Fan, D. Hu, D. Zhang, A.S. Khan, M. Usman, L. Pan, Hierarchical macro-/meso-/microporous oxygen-doped carbon derived from sodium alginate: a cost-effective biomass material for binder-free supercapacitors, Mater. Des. 182 (2019) 108048.
[8] P. Du, L. Liu, Y. Dong, W. Li, J. Li, Z. Liu, X. Wang, Synthesis of hierarchically porous boron-doped carbon material with enhanced surface hydrophobicity and porosity for improved supercapacitor performance, Electrochim. Acta 370 (2021) 137801.
[9] N. Talreja, S. Jung, L.T.H. Yen, T. Kim, Phenol-formaldehyde-resin-based activated carbons with controlled pore size distribution for high-performance supercapacitors, Chem. Eng. J. 379 (2020) 122332.
[10] L. Miao, D. Zhu, Y. Zhao, M. Liu, H. Duan, W. Xiong, Q. Zhu, L. Li, Y. Lv, L. Gan, Design of carbon materials with ultramicro-, supermicro- and mesopores using solvent- and self-template strategy for supercapacitors, Microporous Mesoporous Mater. 253 (2017) 1–9.
[11] M. Yang, Z. Zhou, Recent breakthroughs in supercapacitors boosted by nitrogen-rich porous carbon materials, Adv. Sci. 4 (8) (2017) 1600408.
[12] D. Zhu, K. Cheng, Y. Wang, D. Sun, L. Gan, T. Chen, J. Jiang, M. Liu, Nitrogen–doped porous carbons with nanofiber-like structure derived from poly (aniline-co-p-phenylenediamine) for supercapacitors, Electrochim. Acta 224 (2017) 17–24.
[13] S. Malmberg, M. Arulepp, N. Savest, E. Tarasova, V. Vassiljeva, I. Krasnou, M. Käärik, V. Mikli, A. Krumme, Directly electrospun electrodes for electrical double-layer capacitors from carbide-derived carbon, J. Electrost. 103 (2020) 103396.
[14] H. Kim, M.E. Fortunato, H. Xu, J.H. Bang, K.S. Suslick, Carbon microspheres as supercapacitors, J. Phy. Chem. C 115 (42) (2011) 20481–20486.
[15] C.Y. Tsai, H.C. Tai, C.A. Su, L.M. Chiang, Y.Y. Li, Activated microporous carbon nanospheres for use in supercapacitors, ACS Appl. Nano Mater. 3 (10) (2020) 10380–10388.
[16] X. Shi, S. Zheng, Z.S. Wu, X. Bao, Recent advances of graphene-based materials for high-performance and new-concept supercapacitors, J. Energy Chem. 27 (1) (2018) 25–42.
[17] J. Yin, W. Zhang, N.A. Alhebshi, N. Salah, H.N. Alshareef, Synthesis strategies of porous carbon for supercapacitor applications, Small Methods 4 (3) (2020) 1900853.
[18] T. Liu, F. Zhang, Y. Song, Y. Li, Revitalizing carbon supercapacitor electrodes with hierarchical porous structures, J. Mater. Chem. A 5 (34) (2017) 17705–17733.
[19] L.L. Zhang, Y. Gu, X.S. Zhao, Advanced porous carbon electrodes for electrochemical capacitors, J. Mater. Chem. A 1 (33) (2013) 9395–9408.
[20] X.Y. Luo, Y. Chen, Y. Mo, A review of charge storage in porous carbon-based supercapacitors, New Carbon Mater. 36 (1) (2021) 49–68.
[21] J. Chmiola, G. Yushin, Y. Gogotsi, C. Portet, P. Simon, P.L. Taberna, Anomalous increase in carbon capacitance at pore sizes less than 1 nanometer, Science 313 (5794) (2006) 1760–1763.
[22] C. Largeot, C. Portet, J. Chmiola, P.L. Taberna, Y. Gogotsi, P. Simon, Relation between the ion size and pore size for an electric double-layer capacitor, J. Am. Chem. Soc. 130 (9) (2008) 2730–2731.
[23] L. Xie, F. Su, L. Xie, X. Guo, Z. Wang, Q. Kong, G. Sun, A. Ahmad, X. Li, Z. Yi, C. Chen, Effect of pore structure and doping species on charge storage mechanisms in porous carbon-based supercapacitors, Mater. Chem. Front. 4 (9) (2020) 2610–2634.
[24] J.G. Wang, H. Liu, H. Sun, W. Hua, H. Wang, X. Liu, B. Wei, One-pot synthesis of nitrogen-doped ordered mesoporous carbon spheres for high-rate and long-cycle life supercapacitors, Carbon 127 (2018) 85–92.
[25] Y. Chen, X. Qiu, L.Z. Fan, Nitrogen-rich hierarchically porous carbon foams as high-performance electrodes for lithium-based dual-ion capacitor, J. Energy Chem. 48 (2020) 187–194.
[26] Y. Lin, Z. Chen, C. Yu, W. Zhong, Facile synthesis of high nitrogen-doped content, mesopore-dominated biomass-derived hierarchical porous graphitic carbon for high performance supercapacitors, Electrochim. Acta 334 (2020) 135615.

[27] N. Deka, J. Barman, S. Kasthuri, V. Nutalapati, G.K. Dutta, Transforming waste polystyrene foam into N-doped porous carbon for capacitive energy storage and deionization applications, Appl. Surf. Sci. 511 (2020) 145576.
[28] N.D. Kim, W. Kim, J.B. Joo, S. Oh, P. Kim, Y. Kim, J. Yi, Electrochemical capacitor performance of N-doped mesoporous carbons prepared by ammoxidation, J. Power Sources 180 (1) (2008) 671–675.
[29] H. Chen, M. Zhou, Z. Wang, S. Zhao, S. Guan, Rich nitrogen-doped ordered mesoporous phenolic resin-based carbon for supercapacitors, Electrochim. Acta 148 (2014) 187–194.
[30] M.K. Sahoo, P. Gogoi, G. Rajeshkhanna, S.V. Chilukuri, G.R. Rao, Significance of optimal N-doping in mesoporous carbon framework to achieve high specific capacitance, Appl. Surf. Sci. 418 (2017) 40–48.
[31] A. Ilnicka, J.P. Lukaszewicz, Marine and freshwater feedstocks as a precursor for nitrogen-containing carbons: a review, Mar. Drugs 16 (5) (2018) 142.
[32] H. Wang, Y. Shao, S. Mei, Y. Lu, M. Zhang, J.-k. Sun, K. Matyjaszewski, M. Antonietti, J. Yuan, Polymer-derived heteroatom-doped porous carbon materials, Chem. Rev. 120 (17) (2020) 9363–9419.
[33] A.N. Arias, J. Villarroel-Rocha, K. Sapag, M.F. Mori, G.A. Planes, A.Y. Tesio, V. Flexer, High nitrogen content carbons: morphological and chemical changes with synthesis temperature and application in lithium–sulfur batteries, Electrochim. Acta 359 (2020) 136942.
[34] G. Xu, B. Ding, P. Nie, L. Shen, J. Wang, X. Zhang, Porous nitrogen-doped carbon nanotubes derived from tubular polypyrrole for energy-storage applications, Chem. Eur. J. 19 (37) (2013) 12306–12312.
[35] W. Shen, W. Fan, Nitrogen-containing porous carbons: synthesis and application, J. Mater. Chem. A 1 (4) (2013) 999–1013.
[36] N. Sazali, The influence of carbonization temperature and heating rate towards carbon membrane performance: a review, J. Adv. Res. Fluid Mech. Therm. Sci. 62 (2) (2019) 151–158.
[37] N. Brun, S.A. Wohlgemuth, P. Osiceanu, M.M. Titirici, Original design of nitrogen-doped carbon aerogels from sustainable precursors: application as metal-free oxygen reduction catalysts, Green Chem. 15 (9) (2013) 2514–2524.
[38] M. Thommes, K. Kaneko, A. Neimark, J. Olivier, F. Rodriguez-Reinoso, J. Rouquerol, K. Sing, Physisorption of gases, with special reference to the evaluation of surface area and pore size distribution (IUPAC Technical Report), Pure Appl. Chem. 87 (2015).
[39] S. Brunauer, P.H. Emmett, E. Teller, Adsorption of Gases in multimolecular layers, J. Am. Chem. Soc. 60 (2) (1938) 309–319.
[40] M. Kruk, M. Jaroniec, K.P. Gadkaree, Nitrogen adsorption studies of novel synthetic active carbons, J. Colloid Interface Sci. 192 (1) (1997) 250–256.
[41] J. Villarroel-Rocha, D. Barrera, K. Sapag, Introducing a self-consistent test and the corresponding modification in the Barrett, Joyner and Halenda method for pore-size determination, Microporous Mesoporous Mater. 200 (2014) 68–78.
[42] G. Horváth, K. Kawazoe, Method for the calculation of effective pore size distribution in molecular sieve carbon, J. Chem. Eng. Jpn. 16 (6) (1983) 470–475.
[43] Z. Xu, Y. Li, D. Li, D. Wang, J. Zhao, Z. Wang, M.N. Banis, Y. Hu, H. Zhang, N-enriched multilayered porous carbon derived from natural casings for high-performance supercapacitors, Appl. Surf. Sci. 444 (2018) 661–671.
[44] R. Vicentini, L.M. Da Silva, E.P. Cecilio Junior, T.A. Alves, W.G. Nunes, H. Zanin, How to measure and calculate equivalent series resistance of electric double-layer capacitors, Molecules 24 (8) (2019) 1452.
[45] K.B. Li, D.W. Shi, Z.Y. Cai, G.L. Zhang, Q.A. Huang, D. Liu, C.P. Yang, Studies on the equivalent serial resistance of carbon supercapacitor, Electrochim. Acta 174 (2015) 596–600.
[46] M. Sevilla, W. Gu, C. Falco, M.M. Titirici, A.B. Fuertes, G. Yushin, Hydrothermal synthesis of microalgae-derived microporous carbons for electrochemical capacitors, J. Power Sources 267 (2014) 26–32.
[47] R.W. Pekala, Organic aerogels from the polycondensation of resorcinol with formaldehyde, J. Mater. Sci. 24 (9) (1989) 3221–3227.
[48] Z. Borislav, Č. Jiří, Š. Martin, J. Josef, Pore classification in the characterization of porous materials: a perspective, Open Chem. 5 (2) (2007) 385–395.
[49] C. Shao, S. Qiu, H. Chu, Y. Zou, C. Xiang, F. Xu, L. Sun, Nitrogen-doped porous microsphere carbons derived from glucose and aminourea for high-performance supercapacitors, Catal. Today 318 (2018) 150–156.
[50] A. Bianco, Y. Chen, E. Frackowiak, M. Holzinger, N. Koratkar, V. Meunier, S. Mikhailovsky, M. Strano, J.M.D. Tascon, M. Terrones, Carbon science perspective in 2020: current research and future challenges, Carbon 161 (2020) 373–391.
[51] X. Han, H. Jiang, Y. Zhou, W. Hong, Y. Zhou, P. Gao, R. Ding, E. Liu, A high performance nitrogen-doped porous activated carbon for supercapacitor derived from pueraria, J. Alloys Compd. 744 (2018) 544–551.
[52] L.N. Kong, W. Yang, L. Su, S.G. Hao, G.J. Shao, X.J. Qin, Nitrogen-doped 3D web-like interconnected porous carbon prepared by a simple method for supercapacitors, Ionics 25 (9) (2019) 4333–4340.
[53] J. Wei, D. Zhou, Z. Sun, Y. Deng, Y. Xia, D. Zhao, A Controllable synthesis of rich nitrogen-doped ordered mesoporous carbon for CO_2 capture and supercapacitors, Advanced Functional Materials 23 (18) (2013) 2322–2328.
[54] H. Gul, A.u.H.A. Shah, S. Bilal, Achieving ultrahigh cycling stability and extended potential window for supercapacitors through asymmetric combination of conductive polymer nanocomposite and activated carbon, Polymers 11 (10) (2019) 1678.
[55] K.S. Kim, S.J. Park, Synthesis of nitrogen doped microporous carbons prepared by activation-free method and their high electrochemical performance, Electrochim. Acta 56 (27) (2011) 10130–10136.
[56] J. Du, L. Liu, Y. Yu, Y. Zhang, A. Chen, Monomer self-deposition for ordered mesoporous carbon for high-performance supercapacitors, ChemSusChem 12 (11) (2019) 2409–2414.
[57] L. Zhang, G. Shi, Preparation of highly conductive graphene hydrogels for fabricating supercapacitors with high rate capability, J. Phys. Chem. C 115 (34) (2011) 17206–17212.
[58] F. Md Jamil, M.A. Sulaiman, S. Mohd Ibrahim, A.K. Masrom, M.Z.A. Yahya, Effects of different electrolyte concentrations and scan rates in mesoporous carbon electrode-based capacitance, Adv. Mater. Res. 1133 (2016) 3–7.
[59] M.D. Stoller, R.S. Ruoff, Best practice methods for determining an electrode material's performance for ultracapacitors, Energy Environ. Sci. 3 (9) (2010) 1294–1301.